

The *RON1/FRY1/SAL1* Gene Is Required for Leaf Morphogenesis and Venation Patterning in *Arabidopsis*^{1[W][OA]}

Pedro Robles, Delphine Fleury², Héctor Candela, Gerda Cnops, María Magdalena Alonso-Peral³, Sylvester Anami, Andrea Falcone, Camila Caldana, Lothar Willmitzer, María Rosa Ponce, Mieke Van Lijsebettens, and José Luis Micol*

División de Genética and Instituto de Bioingeniería, Universidad Miguel Hernández, Campus de Elche, 03202 Elche, Alicante, Spain (P.R., H.C., M.M.A.-P., M.R.P., J.L.M.); Department of Plant Systems Biology, Flanders Interuniversity Institute for Biotechnology, and Department of Plant Biotechnology and Genetics, Ghent University, B-9052 Ghent, Belgium (D.F., G.C., S.A., A.F., M.V.L.); and Max-Planck-Institute of Molecular Plant Physiology, D-14476 Potsdam-Golm, Germany (C.C., L.W.)

To identify genes involved in vascular patterning in *Arabidopsis* (*Arabidopsis thaliana*), we screened for abnormal venation patterns in a large collection of leaf shape mutants isolated in our laboratory. The *rotunda1-1* (*ron1-1*) mutant, initially isolated because of its rounded leaves, exhibited an open venation pattern, which resulted from an increased number of free-ending veins. We positionally cloned the *RON1* gene and found it to be identical to *FRY1/SAL1*, which encodes an enzyme with inositol polyphosphate 1-phosphatase and 3'(2'),5'-bisphosphate nucleotidase activities and has not, to our knowledge, previously been related to venation patterning. The *ron1-1* mutant and mutants affected in auxin homeostasis share perturbations in venation patterning, lateral root formation, root hair length, shoot branching, and apical dominance. These similarities prompted us to monitor the auxin response using a *DR5-GUS* auxin-responsive reporter transgene, the expression levels of which were increased in roots and reduced in leaves in the *ron1-1* background. To gain insight into the function of *RON1/FRY1/SAL1* during vascular development, we generated double mutants for genes involved in vein patterning and found that *ron1* synergistically interacts with *auxin resistant1* and *hemivenata-1* but not with *cotyledon vascular pattern1* (*cop1*) and *cop2*. These results suggest a role for inositol metabolism in the regulation of auxin responses. Microarray analysis of gene expression revealed that several hundred genes are misexpressed in *ron1-1*, which may explain the pleiotropic phenotype of this mutant. Metabolomic profiling of the *ron1-1* mutant revealed changes in the levels of 38 metabolites, including myoinositol and indole-3-acetonitrile, a precursor of auxin.

During the vegetative development of *Arabidopsis* (*Arabidopsis thaliana*), leaves are produced from the shoot apical meristem in an orchestrated program that

involves patterning and cell division, expansion, and differentiation. The mature vegetative leaves of *Arabidopsis* are histologically simple and consist of the outer epidermis and internal mesophyll and vasculature (Tsukaya, 2005). Veins are crucial for normal leaf function, transporting water, minerals, and photosynthate and providing mechanical support to the lamina (Evert and Eichhorn, 2006). The leaves of many vascular plants, such as the angiosperms, exhibit a closed reticulate venation pattern (Roth-Nebelsick et al., 2001). In *Arabidopsis*, the leaf venation pattern is brochidodromous, with a single primary vein (midvein) and a series of loops formed by secondary veins that connect other secondary and higher order veins (Hickey, 1973; Candela et al., 1999).

Vein differentiation must be spatially and temporally regulated throughout leaf development. Many aspects of venation patterning in plant leaves can be explained by the auxin canalization model (Sachs, 1991; Rolland-Lagan and Prusinkiewicz, 2005), which is supported by considerable experimental evidence. The role of auxin in venation pattern formation is supported by the phenotypes of mutants possessing altered auxin biosynthesis or perception (Alonso-Peral

¹ This work was supported by the Ministerio de Educación y Ciencia of Spain (grant nos. BFU2005-01031 and BIO2008-04075 as well as a Ph.D. scholarship to M.M.A.-P.), by the European Research Training Network (grant no. HPRN-CT-2002-00267 DAGOLIGN), by the Vlaamse Interuniversitaire Raad (Ph.D. scholarship to S.A.), and by the European Commission (grant nos. HPMT-CT-2000-00088 to A.F. as part of the PREDEC project and LSHG-CT-2006-037704).

² Present address: Australian Centre for Plant Functional Genomics, University of Adelaide, PMB1, Glen Osmond, South Australia 5064, Australia.

³ Present address: Australian National University, Canberra, Australian Capital Territory 0200, Australia.

* Corresponding author; e-mail jlmicol@umh.es.

The author responsible for distribution of materials integral to the findings presented in this article in accordance with the policy described in the Instructions for Authors (www.plantphysiol.org) is: José Luis Micol (jlmicol@umh.es).

^[W] The online version of this article contains Web-only data.

^[OA] Open Access articles can be viewed online without a subscription.

www.plantphysiol.org/cgi/doi/10.1104/pp.109.149369

et al., 2006; Cheng et al., 2006), experimental perturbation of auxin transport (Mattsson et al., 1999; Sieburth, 1999), and the expression pattern of auxin-responsive reporter transgenes (Mattsson et al., 2003; Scarpella et al., 2006). The phenotypes of mutants impaired in auxin transport, such as *scarface* (*sfc*; Deyholos et al., 2000; Sieburth et al., 2006) and *pin-formed1* (*pin1*; Okada et al., 1991; Gälweiler et al., 1998), and perception, such as *monopteros* (*mp*; Hardtke and Berleth, 1998), are pleiotropic and include defects in vein patterning or differentiation. The *sfc* mutant exhibits a disconnected venation pattern (Deyholos et al., 2000), and the lateral organs of strong *mp* mutants display a reduced venation pattern with no peripheral veins (Przemeck et al., 1996). In contrast, the leaf venation pattern of *pin1* mutants resembles that of wild-type plants treated with auxin transport inhibitors, exhibiting extra primary and secondary veins and an accumulation of vascular elements along the leaf margin (Mattsson et al., 1999).

Unlike *sfc*, *pin1*, or *mp*, other leaf venation mutants are not primarily affected in auxin production, perception, or transport (Carland et al., 1999). Examples include *cotyledon vascular pattern1* (*cvp1*), the cotyledons of which exhibit isolated patches of vascular tissue (Carland et al., 1999, 2002), and *cvp2*, which exhibits increased numbers of free-ending veins in the cotyledons and leaves (Carland et al., 1999; Carland and Nelson, 2004). *CVP1* encodes the STEROL METHYLTRANSFERASE2 (SMT2) protein, an enzyme that functions in the sterol biosynthetic pathway (Carland et al., 2002). *CVP2* encodes an inositol polyphosphate 5'-phosphatase (5PTase; Carland and Nelson, 2004), which mediates the hydrolysis of inositol 1,4,5-trisphosphate (IP₃), a eukaryotic second messenger with a pivotal role in calcium signaling (Berridge, 2009). IP₃ controls cytosolic calcium levels by regulating calcium release from the vacuole and endoplasmic reticulum (Krinke et al., 2007). The disconnected, open venation pattern of *cvp2* cotyledons and leaves suggested a role for intracellular IP₃ levels in vascular development (Carland and Nelson, 2004). Recently, *CVP2* and another 5PTase, *CVP2-LIKE1* (*CVL1*), have been shown to regulate vein patterning through the production of a specific phosphoinositide (PI) that acts as a ligand for SFC/VASCULAR NETWORK3 (VAN3), which in turn controls the traffic of vesicles that accounts for the polar subcellular localization of PIN1 proteins (Carland and Nelson, 2009; Naramoto et al., 2009). Another inositol 5PTase, *At5PTase13*, has been shown to play a role in auxin-mediated vein development in cotyledons (Lin et al., 2005). Furthermore, the open vein networks present in the leaves of *forked* and *tornado* mutants (Steynen and Schultz, 2003; Cnops et al., 2006) may be due to altered auxin perception or distribution.

To identify genes required for venation patterning, we screened for naturally occurring variations in the venation pattern of Arabidopsis vegetative leaves (Candela et al., 1999). In this way, we discovered the

spontaneously occurring *hemivenata-1* (*hve-1*) mutation, which causes a venation pattern that is significantly simpler than those of other wild types, such as Landsberg *erecta* (*Ler*) and Columbia-0 (*Col-0*). We positionally cloned the *HVE* gene, which encodes a CAND1 protein involved in ubiquitin-mediated auxin signaling (Alonso-Peral et al., 2006). To identify additional loci necessary for vascular patterning, we screened for venation pattern defects in a collection of leaf shape mutants isolated in our laboratory after ethyl methanesulfonate (EMS) mutagenesis (Berná et al., 1999) and found that the *rotunda1-1* (*ron1-1*) mutant, named after the round laminae of its vegetative leaves, displays disconnected leaf veins. Here, we describe the phenotypic characterization of the *ron1-1* mutant and the map-based cloning of *RON1*, which encodes an inositol polyphosphate 1-phosphatase that plays a role in venation patterning, as determined by morphological, reporter gene, and double mutant analyses. Our results suggest an interplay between inositol and auxin signaling in a number of developmental pathways, including those responsible for leaf venation pattern formation.

RESULTS

Effects of the *ron1-1* Mutation on Leaf Development

To gain insight into the developmental basis of the phenotype caused by the *ron1-1* recessive mutation (Fig. 1), we studied cotyledons and first- and third-

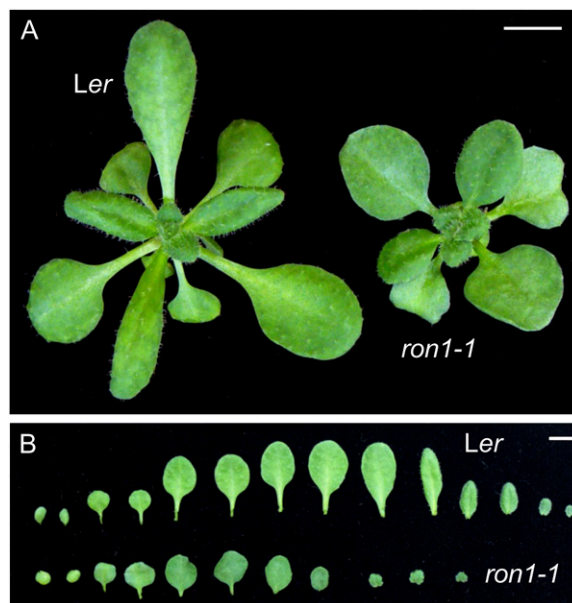


Figure 1. The visible vegetative phenotype of *ron1-1*. A, Basal rosettes of wild-type *Ler* and *ron1-1* mutant plants. B, Cotyledons and leaves excised from *Ler* and *ron1-1* rosettes. The two cotyledons are shown on the left, followed by the vegetative leaves in the order that they initiated. A number of leaves are not fully expanded, given that photographs were taken at 21 DAS. Bars = 5 mm.

node vegetative leaves 22 d after stratification (DAS), which were found to be shorter and wider in the mutant than in the wild type (Table I). These changes translated into length-width ratios close to 1 for all organs examined in *ron1-1*, ranging from 0.95 ± 0.05 in third leaves to 1.11 ± 0.16 in cotyledons. In the *Ler* wild type, the first leaves were the most rounded, with a length-width ratio of 1.17 ± 0.07 . We measured the area of individual palisade cells in the first leaves, which were 42.05% larger in *ron1-1* ($1,617.10 \pm 698.81 \mu\text{m}^2$, $n = 337$) than in *Ler* ($1,138.41 \pm 617.95 \mu\text{m}^2$, $n = 473$; $P = 0$), suggesting that the *RON1* gene restricts cell expansion.

We next characterized the venation pattern of cotyledons and leaves (Fig. 2) using two parameters that quantitatively describe venation pattern complexity: venation density, expressed as the ratio of vein length to leaf area (mm mm^{-2}), and the number of branching points per unit leaf area (Candela et al., 1999). Both parameters demonstrated significantly reduced values in *ron1-1* first leaves but not in cotyledons and third leaves (Fig. 2; Table II). In addition, leaves exhibited more free-ending veins per unit venation length in *ron1-1* than in *Ler* (Table II), indicating altered vein connectivity. Vein disconnections are obvious at the leaf margins and in the apical zone of cleared *ron1-1* leaves. In wild-type leaves, the midvein and two secondary veins usually merged at the leaf apex to form two closed loops (areoles) and an apical hydathode. In contrast, in *ron1-1* leaves, these loops were often incompletely closed (Fig. 3, A and B).

To trace the defects of *ron1-1* mutant leaves to earlier stages, we used an *ATHB-8-GUS* transgene as a reporter of the procambial cells that will differentiate into veins (Baima et al., 1995). The *ATHB-8-GUS* reporter revealed a closed reticulate expression pattern that began during early stages of wild-type leaf development (Fig. 3C). In *ron1-1* leaves, *ATHB-8-GUS* revealed an open network with supernumerary free-ending veins, suggesting that fewer cells had been recruited to a vascular fate, particularly near the leaf margins (Fig. 3D). This defect was observed in developing first leaves, which had the simplest venation patterns, as well as in leaves produced later in development (Fig. 3, G and H). The closed *ATHB-8-GUS* expression patterns observed early in wild-type leaf

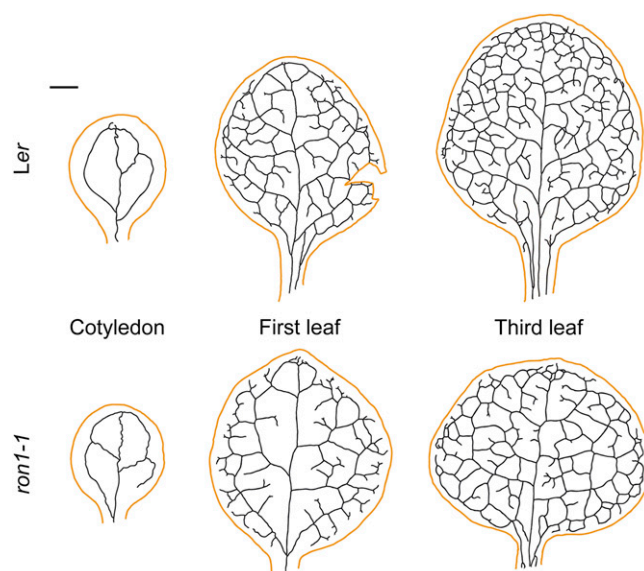


Figure 2. Cotyledon and leaf venation patterns in *ron1-1*. Diagrams were drawn on micrographs taken from cleared cotyledons and leaves. Organ margins and vascular strands are represented in orange and black, respectively. Plant material was collected at 22 DAS. Bar = 1 mm.

primordia correlated with a closed venation pattern in cleared mature leaves (Fig. 3E), and the aberrant *ATHB-8-GUS* expression patterns observed in young *ron1-1* leaf primordia correlated with partially open venation patterns and with the disconnected secondary veins near the leaf margins in mature leaves (Fig. 3F).

Other Pleiotropic Effects of the *ron1-1* Mutation

Other morphological defects were apparent in *ron1-1* roots and shoots. When grown in vertically oriented petri dishes, fewer lateral roots developed in *ron1-1* (18.77 ± 5.73 , $n = 18$) than in *Ler* (31.91 ± 11.54 , $n = 32$; $P = 8.58 \times 10^{-10}$; Fig. 4A), and the primary roots of 14-DAS seedlings were similar in length in *Ler* (5.87 ± 1.09 cm, $n = 15$) and *ron1-1* (5.47 ± 0.68 cm, $n = 20$; $P = 0.217$). Root hairs were approximately four times longer in the mutant ($386.17 \pm 137.14 \mu\text{m}$, $n = 23$) than in the wild type ($119.04 \pm 17.48 \mu\text{m}$, $n = 23$; $P = 6.62 \times$

Table I. Morphometric analysis of the lamina of *ron1-1* cotyledons and vegetative leaves

All values are means \pm SD. Values significantly different from those of *Ler* ($P \leq 0.05$) are indicated in italics.

| Organ | Line | Length | Width | Length-Width Ratio | Area | <i>n</i> |
|------------|---------------|-----------------|-----------------|-----------------------------------|------------------------|----------|
| | | <i>mm</i> | <i>mm</i> | | <i>mm</i> ² | |
| Cotyledon | <i>Ler</i> | 3.70 ± 0.52 | 2.97 ± 0.43 | 1.25 ± 0.09 | 10.20 ± 2.61 | 9 |
| | <i>ron1-1</i> | 3.28 ± 0.51 | 3.64 ± 0.73 | <i>1.11 ± 0.16</i> | 11.23 ± 3.41 | 8 |
| First leaf | <i>Ler</i> | 5.87 ± 1.00 | 5.01 ± 0.72 | 1.17 ± 0.07 | 27.03 ± 8.18 | 9 |
| | <i>ron1-1</i> | 5.62 ± 0.63 | 5.33 ± 0.50 | <i>1.05 ± 0.07</i> | 27.08 ± 5.36 | 9 |
| Third leaf | <i>Ler</i> | 6.94 ± 1.14 | 5.59 ± 0.86 | 1.24 ± 0.09 | 34.07 ± 8.31 | 7 |
| | <i>ron1-1</i> | 5.72 ± 0.82 | 6.03 ± 0.91 | <i>0.95 ± 0.05</i> | 31.94 ± 8.18 | 9 |

Table II. Morphometric analysis of the venation pattern of *ron1-1*All values are means \pm sd. Values significantly different from those of *Ler* ($P \leq 0.05$) are indicated in italics.

| Organ | Line | Area | Venation Length | Venation Density | No. of Branching Points | No. of Branching Points per mm ² | No. of Free-Ending Veins | No. of Free-Ending Veins per Venation Length (mm) | <i>n</i> |
|------------|---------------|------------------|--------------------|---------------------|-------------------------|---|--------------------------|---|----------|
| | | mm ² | mm | mm mm ⁻² | | | | | |
| Cotyledon | <i>Ler</i> | 10.20 \pm 2.61 | 16.17 \pm 2.43 | 1.63 \pm 0.21 | 6.56 \pm 0.73 | 0.68 \pm 0.19 | 1.11 \pm 1.05 | 0.07 \pm 0.06 | 9 |
| | <i>ron1-1</i> | 11.23 \pm 3.41 | 16.56 \pm 3.96 | 1.51 \pm 0.21 | 7.50 \pm 2.39 | 0.70 \pm 0.29 | 2.13 \pm 0.99 | 0.13 \pm 0.07 | 8 |
| First leaf | <i>Ler</i> | 27.03 \pm 8.18 | 84.82 \pm 23.46 | 3.16 \pm 0.15 | 122.56 \pm 39.95 | 4.60 \pm 0.62 | 48.22 \pm 14.54 | 0.58 \pm 0.13 | 9 |
| | <i>ron1-1</i> | 27.08 \pm 5.36 | 67.50 \pm 18.19 | 2.47 \pm 0.29 | 96.22 \pm 32.28 | 3.49 \pm 0.76 | 58.44 \pm 19.57 | 0.85 \pm 0.11 | 9 |
| Third leaf | <i>Ler</i> | 34.07 \pm 8.31 | 144.74 \pm 32.69 | 4.28 \pm 0.34 | 270.71 \pm 62.04 | 8.04 \pm 1.24 | 79.00 \pm 16.27 | 0.55 \pm 0.09 | 7 |
| | <i>ron1-1</i> | 31.95 \pm 8.18 | 124.17 \pm 19.12 | 4.05 \pm 0.86 | 240.78 \pm 49.28 | 8.11 \pm 2.91 | 92.22 \pm 13.13 | 0.75 \pm 0.13 | 9 |

10⁻¹²; Fig. 4, B and C). In addition, the *ron1-1* mutant bolted late (34.56 \pm 0.88 DAS, $n = 9$) compared with *Ler* (28.90 \pm 1.20 DAS, $n = 10$; $P = 0$; Fig. 4D), and its main inflorescence was shorter (16.52 \pm 1.27 cm, $n = 20$) than that of the wild type (25.29 \pm 1.75 cm, $n = 20$; $P = 2.79 \times 10^{-20}$). Late flowering was associated with a higher number of rosette leaves in *ron1-1* (13.78 \pm 1.20, $n = 9$) than in *Ler* (11.9 \pm 1.20, $n = 10$; $P = 0.003$) at the time of bolting. Consistent with a loss of apical dominance, more secondary inflorescences developed in *ron1-1* (5.60 \pm 0.97, $n = 10$) than in *Ler* (3.07 \pm 0.62, $n = 14$; $P = 8.14 \times 10^{-8}$; Fig. 4E).

Map-Based Cloning of *RON1*

The *ron1-1* mutation was initially mapped to chromosome 5 (Robles and Micol, 2001) and then further narrowed down to a 455-kb interval defined by amplified fragment length polymorphism markers (SM141_73.2 and SM15_273.7; Peters et al., 2004; Fig. 5). Recombinants were used for fine-mapping and delineated the locus to 157- and 30-kb intervals flanked by insertion/deletion (CER455741 and CER457062) and single-nucleotide polymorphism (CER455210 and CER436450) markers, respectively (Supplemental Table S1). The seven genes within the 30-kb interval (At5g63940, At5g63950, At5g63960, At5g63970, At5g63980, At5g63990, and At5g64000) were sequenced for both *ron1-1* and *Ler* (Supplemental Table S2). Consistent with the lesions usually caused by EMS, a G-to-A transition mutation was found in the At5g63980 transcription unit. Analysis of a CAP3 (Huang and Madan, 1999) assembly of cDNA sequences available in GenBank indicated that the open reading frame of the At5g63980 gene, also known as *FIERY1* (*FRY1*; Xiong et al., 2001), *SAL1* (Quintero et al., 1996), *HIGH EXPRESSION OF OSMOTICALLY RESPONSIVE GENES2* (*HOS2*; Xiong et al., 2004), and *ALTERED EXPRESSION OF APX2 8* (*ALX8*; Wilson et al., 2009), comprises 407 amino acids. This open reading frame has previously been shown to encode inositol polyphosphate 1-phosphatase and 3'(2'),5'-bisphosphate nucleotidase activities (Quintero et al., 1996; Xiong et al., 2001).

The expression pattern of *RON1/FRY1* has been previously determined by northern-blot and promoter-

GUS fusion analyses (Xiong et al., 2001). *RON1/FRY1* is expressed in the primary root and root hairs as well as the leaves, stems, and flowers. The highest expression signal detected in the leaves occurs in the veins. We analyzed *RON1* expression in silico using Genevestigator (Zimmermann et al., 2005) and found the gene to be expressed almost ubiquitously, except in the stigmata and in pollen, and throughout development, with the highest levels observed in young seedlings

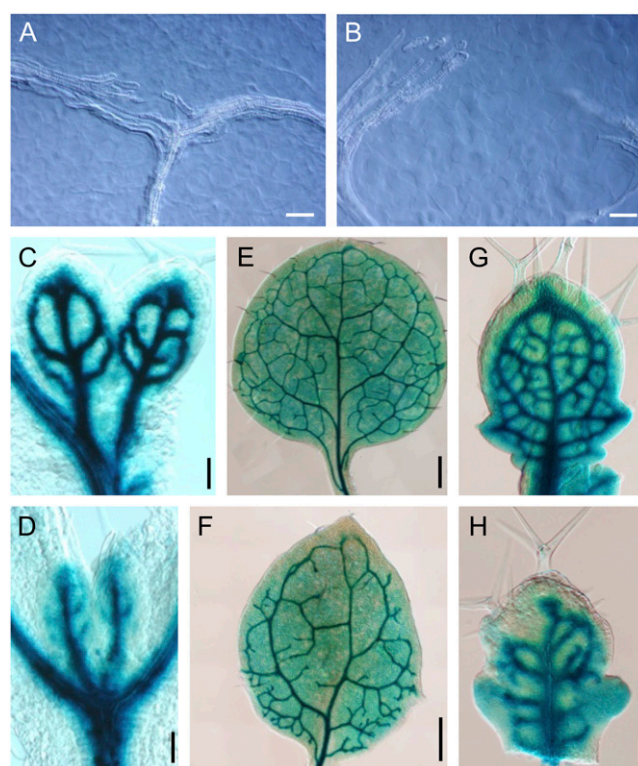


Figure 3. Decreased connectivity in *ron1-1* leaf veins. A and B, Vascular strands from the apex of *Ler* (A) and *ron1-1* (B) first-node leaves. C to H, GUS activity in leaves obtained from the first two nodes (C–F) and the fifth node (G and H) of *ATHB-8-GUS* transgenic plants in *Wassilewskija* (C, E, and G) and *ron1-1* (D, F, and H) backgrounds. Interference contrast micrographs were taken at 5 DAS (C and D), 12 DAS (E and F), and 23 DAS (G and H). Bars = 40 μ m (A and B), 50 μ m (C, D, G, and H), and 200 μ m (E and F).

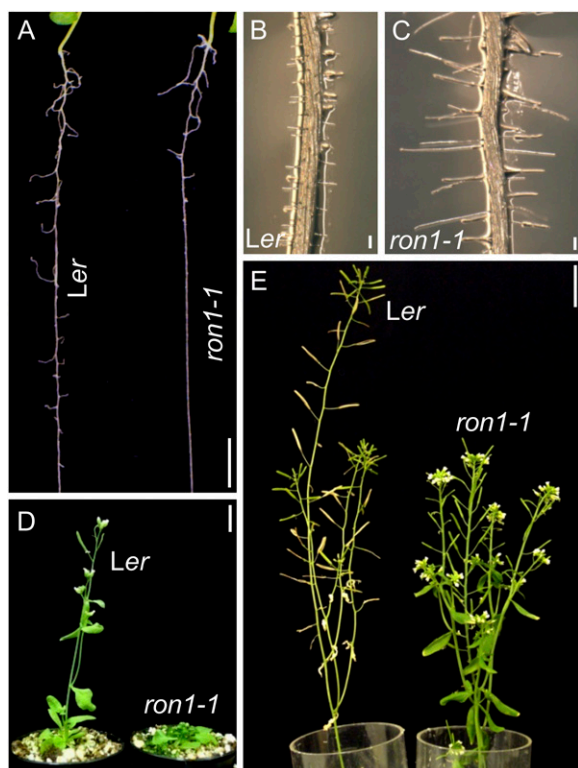


Figure 4. Pleiotropy in the *ron1-1* mutant. A, The number of secondary roots was reduced in *ron1-1*. B and C, Root hairs were longer in *ron1-1* (C) than in *Ler* (B). D, Late flowering (delayed bolting) in *ron1-1*. E, The inflorescence of *ron1-1* was bushier than that of *Ler*. Photographs were taken at 14 DAS (A–C), 31 DAS (D), and 56 DAS (E). Bars = 5 mm (A), 100 μ m (B and C), and 1 cm (D and E).

(1–4 DAS) and during the flowering stages (21–25 DAS). Using Mutant Surveyor in Geneinvestigator, we found that *RON1* is overexpressed (1.3- to 2.7-fold change) in the *continuous vascular ring1* mutant, which is characterized by increased vascular tissue development in the stem (Parker et al., 2003).

The G-to-A substitution in *ron1-1* affects the last nucleotide of the fourth intron in the At5g63980 gene, which damages the splice acceptor site. This suggests that intron splicing is perturbed. We performed reverse transcription (RT)-PCR using primers that anneal to the first and fifth exons of At5g63980 and detected a single band for *Ler* but two bands for *ron1-1*, one of which was slightly smaller and the other larger than that of the wild type (data not shown). Nine nucleotides were absent from the smaller of these mutant transcripts as a consequence of the presence of a cryptic splice site located nine nucleotides downstream of the boundary between the fourth and fifth exons. The absence of these nine nucleotides is predicted to delete three conserved amino acid residues (FLR) present in an α -helix adjacent to the WVLDPIDGT motif (York et al., 1995), which is highly conserved in inositol polyphosphate 1-phosphatases. Intron 4 (119 bp) remained unspliced in the large tran-

script, which encodes a truncated protein in which the active and the substrate-binding sites of the conserved inositol monophosphatase 3'-phosphoadenosine 5'-phosphate (PAP) phosphatase domain are affected. Because normal transcripts were not found, we assumed that the *ron1-1* allele is either hypomorphic or null.

We identified three lines (SALK_020882, SALK_079259, and SALK_005741) carrying T-DNA insertions in At5g63980 (<http://atidb.org/cgi-perl/gbrowse/atibrowse/>), but phenotypically mutant plants were found only among the T4 progeny of SALK_020882. Mutants also appeared in the F1 progeny of a complementation cross between SALK_020882 (in the Col-0 background) and *ron1-1* (*Ler*), confirming that they carry allelic mutations. We PCR amplified and sequenced the genomic region adjacent to the left T-DNA border in SALK_020882 and determined that the T-DNA is inserted immediately upstream of the last nucleotide of exon 3 (Fig. 5). This allele, which had been designated *ron1-2* by us and *fry1-6* by previous authors (Gy et al., 2007), is predicted to yield a truncated protein with 135 amino acids, the first 125 of which are shared with the wild-type *RON1* protein. The absence of most of the PAP phosphatase domain in this protein suggests that *ron1-2* is a null allele. The *ron1-2* mutant showed rounded leaves (Supplemental Fig. S1) and venation pattern defects even stronger than those of *ron1-1*, at least in the first leaf (Table III; see Fig. 7 below).

We examined 16 T-DNA insertion mutants corresponding to four other *Arabidopsis* genes that encode

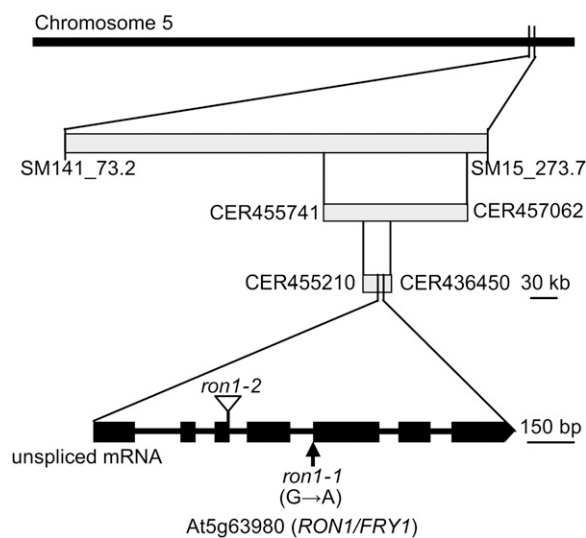


Figure 5. Positional cloning and gene structure of *RON1*. Map-based strategy followed to clone the *ron1-1* mutation is shown. In the representation of the structure of *RON1*, exons are indicated by boxes and introns are indicated by lines between boxes. The *ron1-1* mutation caused a G-to-A substitution at the splice acceptor site of intron 4. The T-DNA insertion in *ron1-2* is represented by an inverted triangle.

Table III. Morphometric analysis of the venation pattern of first-node leaves in double mutants

All values are means \pm sd. In italics, values significantly different from those of Col-0 ($P \leq 0.05$); in boldface, values significantly different from those of *ron1-2* ($P \leq 0.05$); marked by asterisk, values of the double mutants significantly different from those of Col-0 and both single mutants ($P \leq 0.05$).

| Genotype | Area | Venation Length | Venation Density | No. of Branching Points | No. of Branching Points per mm ² | No. of Free-Ending Veins | No. of Free-Ending Veins per Venation Length (mm) | <i>n</i> |
|-----------------------|------------------------------------|-------------------------------------|------------------------------------|--------------------------------------|---|------------------------------------|---|----------|
| | mm ² | mm | mm mm ⁻² | | | | | |
| Col-0 | 35.45 \pm 8.51 | 101.32 \pm 19.53 | 2.90 \pm 0.23 | 107.00 \pm 18.01 | 3.09 \pm 0.40 | 31.3 \pm 6.55 | 0.31 \pm 0.04 | 11 |
| <i>ron1-2</i> | <i>24.81 \pm 2.16</i> | <i>76.83 \pm 9.52</i> | <i>3.09 \pm 0.21</i> | <i>104.00 \pm 19.77</i> | <i>4.17 \pm 0.58</i> | <i>49.9 \pm 12.13</i> | <i>0.65 \pm 0.13</i> | 10 |
| <i>cvp1-3</i> | <i>24.43 \pm 3.41</i> | <i>76.24 \pm 9.72</i> | <i>3.13 \pm 0.23</i> | <i>89.8 \pm 14.54</i> | <i>3.71 \pm 0.61</i> | 24.9 \pm 6.56 | 0.33 \pm 0.08 | 10 |
| <i>ron1-2 cvp1-3</i> | <i>23.14 \pm 5.20</i> | <i>71.99 \pm 12.80</i> | <i>3.16 \pm 0.33</i> | <i>94.4 \pm 16.77</i> | <i>4.23 \pm 0.95</i> | 35.3 \pm 9.30 | 0.50 \pm 0.17* | 10 |
| <i>cvp2-1</i> | <i>27.06 \pm 6.80</i> | <i>78.72 \pm 17.59</i> | <i>2.95 \pm 0.34</i> | <i>89.9 \pm 17.58</i> | 3.44 \pm 0.71 | 76.7 \pm 18.28 | 0.97 \pm 0.11 | 10 |
| <i>ron1-2 cvp2-1</i> | 32.32 \pm 6.68 | <i>81.40 \pm 15.07</i> | <i>2.54 \pm 0.24*</i> | <i>93.1 \pm 20.71</i> | 2.92 \pm 0.52 | 80.2 \pm 15.02 | 0.99 \pm 0.10 | 10 |
| <i>hve-2</i> | 17.02 \pm 5.00 | 35.97 \pm 10.12 | 2.12 \pm 0.11 | 23.8 \pm 6.44 | 1.42 \pm 0.21 | 11.1 \pm 3.18 | 0.32 \pm 0.10 | 10 |
| <i>ron1-2 hve-2</i> | 19.65 \pm 5.30 | 30.58 \pm 8.26 | <i>1.56 \pm 0.18*</i> | <i>19.1 \pm 5.34*</i> | 0.99 \pm 0.25 | <i>17.7 \pm 3.92*</i> | <i>0.60 \pm 0.14</i> | 10 |
| <i>axr1-12</i> | 15.67 \pm 3.59 | 36.33 \pm 8.12 | 2.33 \pm 0.30 | 34.12 \pm 10.38 | 2.21 \pm 0.71 | 17.88 \pm 6.31 | 0.49 \pm 0.13 | 8 |
| <i>ron1-2 axr1-12</i> | <i>7.61 \pm 3.89*</i> | <i>9.75 \pm 7.10*</i> | <i>1.17 \pm 0.38*</i> | <i>6.00 \pm 5.77*</i> | <i>0.51 \pm 0.25*</i> | <i>7.89 \pm 6.05*</i> | <i>0.85 \pm 0.36</i> | 9 |

inositol polyphosphate 1-phosphatases (see "Materials and Methods"): *SAL2* (At5g64000), *SAL3* (At5g63990), *SAL4* (At5g09290), and *AHL* (At5g54390). *SAL2* and *SAL3* are arranged in tandem to *FRY1/RON1* (Xiong et al., 2001). No visible phenotypes were detected in the T3 and T4 generations of these insertion lines, possibly due to functional redundancy between members of the same gene family. In contrast, the unique phenotypes observed in *ron1* mutants demonstrate that *RON1* performs at least some discrete, nonoverlapping functions.

Effects of *ron1* Mutations on Auxin Homeostasis

Venation patterning, lateral root formation, root hair length, shoot branching, and apical dominance, all of which are affected in *ron1* mutants, are processes known to be regulated by auxin (Pitts et al., 1998; Alonso-Peral et al., 2006; De Smet and Jürgens, 2007; Ongaro and Leyser, 2007). To ascertain whether the *ron1-1* mutation affects auxin perception, we monitored the expression pattern of the synthetic auxin reporter *DR5-GUS* (Ulmasov et al., 1997) in different tissues. Consistent with previous results (Sabatini et al., 1999), GUS signal was detected in the columella initial cells, the quiescent center, and the columella root cap of wild-type roots (Fig. 6A). In *ron1-1*, the GUS-staining area was broader in the root tip and often extended to the root vasculature (Fig. 6G), indicating a disrupted pattern of auxin perception or accumulation in roots. In wild-type first leaf primordia, strong *DR5-GUS* expression was detected at the position of the apical hydathode and in the differentiating vascular cells, which were visible as a network (Fig. 6B; Mattsson et al., 2003). In contrast, in *ron1-1* leaf primordia, the signal was consistently reduced compared with the wild type and confined to the apical region (Fig. 6H). As the leaf developed and tracheary elements differentiated distally in wild-type

plants, *DR5-GUS* expression persisted in the apex and appeared as a network only in the proximal portion of the leaf (Fig. 6, C and D). At this stage, however, *DR5-GUS* expression was weak and fuzzy at the basal portion of *ron1-1* leaves and persisted strongly only in the leaf apex (Fig. 6, I and J). Later, close to the end of first leaf expansion, *DR5-GUS* expression appeared along the leaf margin, with maximum levels observed at the leaf apex and the apical and lateral hydathodes in wild-type leaves and, to a much lesser extent, in *ron1-1* leaves (Fig. 6, E and K). A similar decrease in *DR5-GUS* expression levels was observed in leaves from other nodes (Fig. 6, F and L).

To gain insight into the role of *RON1* in auxin homeostasis, we grew mutant and wild-type plants in vertically oriented petri dishes in the presence of different concentrations of the synthetic auxin 2,4-dichlorophenoxyacetic acid (2,4-D) or the auxin efflux inhibitors *N*-1-naphthylphthalamic acid (NPA) and 2,3,5-triiodobenzoic acid (TIBA). The effects of 2,4-D, NPA, and TIBA were similar in *ron1-1* and *Ler*. Growth of *ron1-1* in solid medium supplemented with 0.1 μ M 2,4-D failed to rescue the aberrations in the leaf venation pattern (data not shown). We also tested if auxin responses were reduced in *ron1-1* by applying exogenous auxin (1 μ M indole-3-acetic acid [IAA] or 1 μ M 2,4-D). *ron1-1 DR5-GUS* plants were grown in non-supplemented solid medium for 4 weeks and then incubated for 6 h in liquid medium supplemented with the hormone. We observed a reduced response of the *DR5-GUS* reporter in the leaves of *ron1-1 DR5-GUS* plants compared with the response of a nonmutant control (Supplemental Fig. S2).

Phenotypes of the *ron1 cvp1* and *ron1 cvp2* Double Mutants

CVP2 encodes an inositol polyphosphate 5'-phosphatase, and its loss-of-function mutations determine

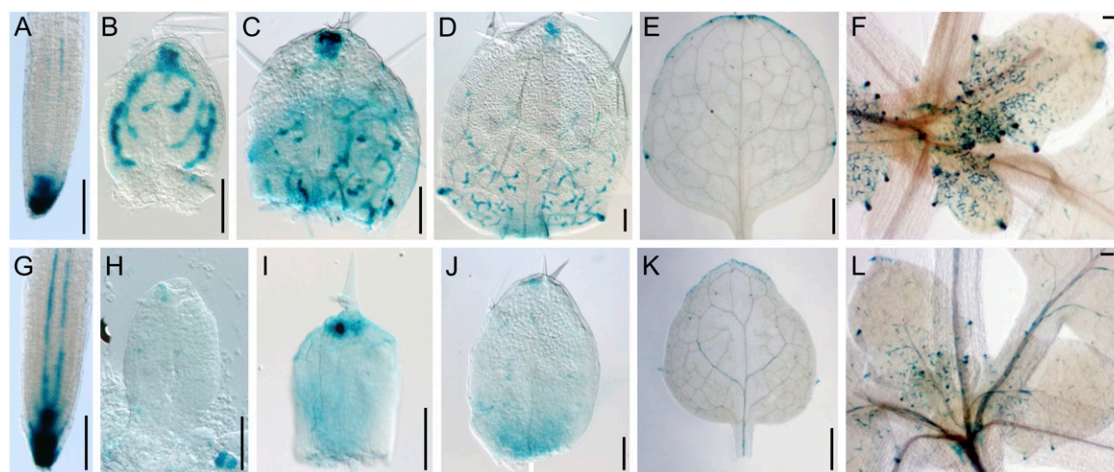


Figure 6. *DR5-GUS* expression in *ron1-1*. Root tips (A and G), first-node leaves (B–E and H–K), and incipient leaves (F and L) of *DR5-GUS* transgenic plants in Col-0 (A–F) and *ron1-1* (G–L; mixed Ler/Col) backgrounds. Photographs were taken at 4 DAS (A and G), 5 DAS (B and H), 7 DAS (C and I), 8 DAS (D and J), and 14 DAS (E, F, K, and L). Bars = 100 μ m (A–D, F–J, and L) and 1 mm (E and K).

an open venation pattern in leaves and cotyledons due to premature vein termination, which affects higher order veins more severely than lower order veins (Carland and Nelson, 2004). Similar vein phenotypes are caused by mutations in *CVP1*, a gene that encodes the sterol methyltransferase *SMT2*, although only in cotyledons, sepals, and petals (Carland et al., 2002). Whole organ morphology is not visibly altered in the leaves of *cvp1* and *cvp2* mutants, which nevertheless exhibit an increased number of free-ending veins and reduced venation complexity, as observed for *ron1-1* (Fig. 7).

To ascertain whether *RON1* is functionally related to *CVP1* or *CVP2*, we crossed *ron1-2* to *cvp2-1* and *cvp1-3*. Only two phenotypic classes were found at a 3:1 (wild

type:*RON1*) ratio in the F2 progeny of these crosses. F3 families were derived from individual *ron1-2* plants and genotyped to assess the presence of a *cvp* mutation. *ron1-2 cvp1-3* and *ron1-2 cvp2-1* double mutants in the Col-0 background had similar morphology to the *ron1-2* single mutant (Supplemental Fig. S3). We measured the venation pattern of first-node leaves from at least 10 plants of each genotype (Table III). Venation density was slightly but significantly reduced in the *ron1-2 cvp2-1* double mutant ($2.54 \pm 0.24 \text{ mm mm}^{-2}$) compared with the single mutants (*ron1-2*, $3.09 \pm 0.21 \text{ mm mm}^{-2}$; *cvp2-1*, $2.95 \pm 0.34 \text{ mm mm}^{-2}$) and the Col-0 wild type ($2.90 \pm 0.23 \text{ mm mm}^{-2}$). This observation suggests that *RON1* and *CVP2* participate in the same process. The number of branching points per

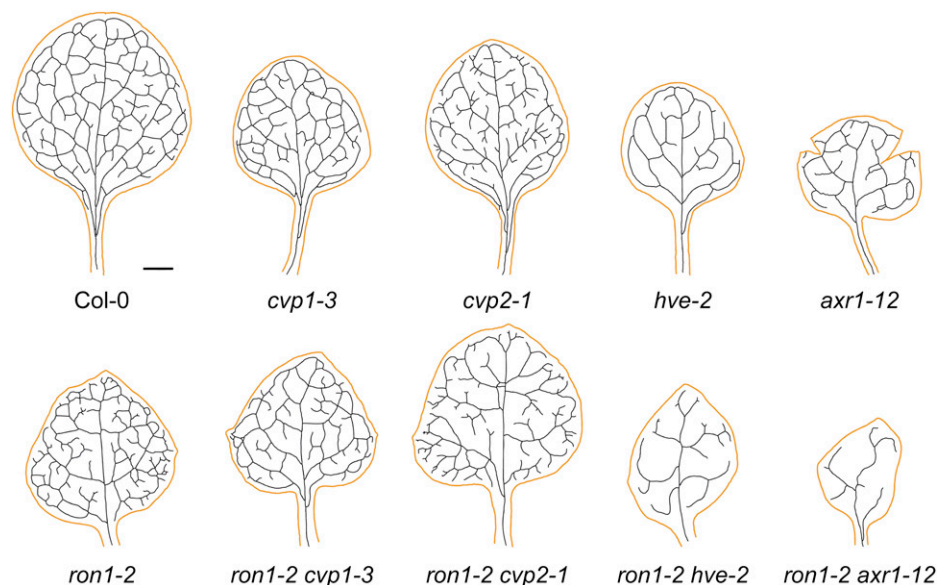


Figure 7. Venation patterns of double mutants involving the *ron1-2* mutation. Venation diagrams were drawn from first-node leaves. Plant material was collected at 21 DAS. Bar = 1 mm.

mm² and the number of free-ending veins per mm of venation were similar in *cvp2-1* (3.44 ± 0.71 and 0.97 ± 0.11 , respectively) and the double mutant (2.92 ± 0.52 and 0.99 ± 0.10), suggesting that the *cvp2-1* mutation is epistatic on *ron1-2* (4.17 ± 0.58 and 0.65 ± 0.13) regarding these venation traits. In contrast, the number of free-ending veins per unit venation length in *ron1-2 cvp1-3* leaves (0.50 ± 0.17) was intermediate to those of *ron1-2* (0.65 ± 0.13) and *cvp1-3* (0.33 ± 0.08), suggesting that *cvp1* suppresses, to some extent, the effects of *ron1-1* on vein connectivity. In agreement with this, the venation pattern of the *ron1-2 cvp1-3* double mutant was less open than that of *ron1-1* (Fig. 7).

The *ron1-2* Mutation Synergistically Interacts with *hve* and *axr1*

The pleiotropic phenotype of *ron1-1* and *ron1-2* and the reduced *DR5-GUS* expression pattern observed in *ron1-1* leaves seemed compatible with a mild auxin perception defect. These observations prompted us to analyze the interactions between *ron1* and other mutants with impaired auxin perception and abnormal venation patterns, such as *auxin resistant1* (*axr1*; Deyholos et al., 2003; Alonso-Peral et al., 2006) and *hve* (Candela et al., 1999; Alonso-Peral et al., 2006; Fig. 7). We obtained double mutant combinations of the *ron1-2*, *axr1-12*, and *hve-2* mutations in the Col-0 background. The *ron1-2 hve-2* and *ron1-2 axr1-12* rosettes were small, particularly in *ron1-2 axr1-12* (Supplemental Fig. S3). The venation pattern defects were also greatly enhanced in the leaves of these double mutants (Fig. 7), especially in *ron1-2 axr1-12*. In this strain, all the morphometric descriptors but one were significantly different from both single mutants and Col-0, suggesting a possible synergistic interaction (Pérez-Pérez et al., 2009). In these double mutants, the venation of first-node leaves was often completely open (Fig. 7) and reduced to a single primary vein with a few secondary veins. In agreement with this reduction in venation pattern complexity, the values obtained for venation density and branching points per mm² in the first-node leaves of these double mutants were similar to, or even lower than, those of *Ler* or *ron1-1* cotyledons (Tables I and III). No closed areoles were observed in 31 of 32 first-node leaves of *ron1-2 axr1-12* plants and five of 20 first-node leaves of *ron1-2 hve-2* plants. The veins of *ron1-2 axr1-12* leaves included parallel vascular strands that often failed to contact each other (data not shown). In addition, the leaves of both double mutants were significantly smaller (Fig. 7) and deeply lobed later in development (Supplemental Fig. S4). The enhanced vein defects and the pronounced lobing of double mutant leaves suggest an interaction between *RON1*, *HVE*, and *AXR1*.

Global Expression Profiling of the *ron1-1* Mutant

A transcriptomic analysis of *ron1-1* shoot apices was carried out using ATH1 microarrays, which demon-

strated 663 genes that were differentially expressed at $P < 0.01$, 392 and 271 of which were up-regulated and down-regulated, respectively (Supplemental Table S3). To validate these results, quantitative (q) RT-PCR analysis of 14 genes selected from among the up-regulated ones was performed. Twelve of these 14 genes were validated by qRT-PCR, confirming the microarray results (Supplemental Tables S4 and S5).

BiNGO (Biological Networks Gene Ontology; Maere et al., 2005) analysis showed that some up-regulated genes participate in developmental processes, such as the determination of symmetry, adaxial/abaxial patterning, primary shoot apical meristem specification, meristem initiation, and root cap development (Fig. 8A; Supplemental Table S6). Other up-regulated genes participate in physiological processes such as amino acid and derivative metabolism, flavonoid synthesis, nitrate assimilation, and basic amino acid transport. This analysis also showed that genes involved in responding to some stimuli (ethylene and metal ion) and to microRNA (miRNA)-mediated gene silencing are overexpressed in *ron1-1*. Indeed, changes in the expression of 24 genes that are known or predicted miRNA targets were detected (Supplemental Table S7). All of them were up-regulated in *ron1-1*, suggesting a defect in miRNA-mediated gene silencing that might be related to the proposed role of *RON1*/*FRY1* as an endogenous RNA-silencing suppressor (Gy et al., 2007). On the other hand, genes related to salinity and cold responses, organic acid biosynthesis, starch catabolism, fatty acid biosynthesis, phagocytosis, and chromatin assembly or disassembly were down-regulated in *ron1-1* (Fig. 8B; Supplemental Table S6).

To ascertain whether hormone-activated developmental pathways are affected in *ron1-1*, we compared our *ron1-1* microarray results with those of Nemhauser et al. (2006; Supplemental Table S8). These authors searched for transcriptional targets of seven plant hormones: abscisic acid (ABA), methyl jasmonate (MJ), auxin, brassinolide (BL), the ethylene precursor 1-aminocyclopropane-1-carboxylic acid, the cytokinin zeatin, and the gibberellin GA₃. The set of genes differentially expressed in the *ron1-1* microarray made up an overrepresented sample of genes that are up-regulated in the presence of ABA, which is in line with the role of *FRY1*/*RON1* in the regulation of ABA responses (Xiong et al., 2001). In addition, a significant number of genes whose expression is deregulated by MJ were up-regulated in *ron1-1*. Indeed, *RON1* itself was found to be specifically regulated by MJ and is considered a marker for this hormone (Nemhauser et al., 2006). To determine if *ron1-1* is affected in the MJ response, we assayed the effects of MJ on the growth of wild-type and *ron1-1* roots. Root growth was slightly more inhibited by 5, 10, and 50 μM MJ in *ron1-1* than in wild-type plants (data not shown). The *ron1-1* microarray data set was also enriched in BL target genes but exhibited expression changes of opposite sign: genes up-regulated by BL were down-regulated in the *ron1-1* mutant, and genes down-regulated by BL were up-

regulated in the *ron1-1* mutant. We studied the effect of BL (25, 50, 100, 300, and 500 μM 24-epibrassinolide) on the growth of *ron1-1* roots, but no effects were detected (data not shown).

The 266 nuclear genes down-regulated in *ron1-1* were analyzed using Athena (O'Connor et al., 2005), and the nine-nucleotide AAAATATCT "evening element" (Harmer et al., 2000) was found to be significantly overrepresented in 39 of them ($P < 10^{-9}$; the P value threshold for significant enrichment is $<10^{-4}$; Supplemental Table S9). The set of genes down-regulated in *ron1-1* was also significantly enriched in nuclear genes encoding chloroplast-targeted proteins (96 of 266 genes; $P < 10^{-10}$; the P value threshold for significant enrichment in Gene Ontology terms is $<10^{-6}$; Supplemental Table S10), 15 of which contained the evening element in their promoters. It is known that the evening element is essential for circadian rhythmicity and that nuclear genes encoding plastid proteins are coregulated by the circadian clock, which helps plants become more efficient in using solar energy (Harmer et al., 2000).

Metabolic Profiling of the *ron1-1* Mutant

To characterize the metabolic changes that are caused by the *ron1-1* mutation, the metabolomes of *ron1-1* and *Ler* were compared using gas chromatography-mass spectrometry (GC-MS). Over 80 metabolites were detected, but only those showing significant changes (i.e. false discovery rate < 0.05 and absolute fold change higher than 1.2) were used for subsequent comparison. The levels of 21 metabolites were significantly increased in *ron1-1*, whereas those of 17 metabolites were decreased when compared with *Ler* (Supplemental Table S11; Supplemental Fig. S5). These included sugars, amino acids, non-tricarboxylic acid cycle organic acids, and other unknown compounds. The levels of myoinositol, an intermediate of inositol metabolism, were significantly changed in *ron1-1* (1.3-fold), which may be related to altered inositol metabolism. Although the biosynthesis of auxin can be dependent on Trp, the levels of this amino acid did not change in *ron1-1*. However, appreciable levels of the related compound indole-3-acetonitrile, a precursor of IAA in one of the Trp-dependent auxin biosynthesis pathways, were up-regulated in the mutant (2.6-fold). The induction of myoinositol and indole-3-acetonitrile may suggest that *RON1* is an interplayer between inositol and auxin signaling. Variation in the levels of several amino acids was detected in the *ron1-1* mutant.

Decreased levels were consistently detected in *ron1-1* for several sugars, including Fru, Glc, sorbose, and altrose. Similar changes in sugar metabolism had been recently observed in the *fry1-1* mutant, suggesting a role for *RON1* in transient starch accumulation and osmotic stress protection (Wilson et al., 2009). We detected in addition higher levels of trehalose and precursors of polyamine biosynthesis in *ron1-1* leaves.

DISCUSSION

In a screen for EMS-induced leaf shape mutants in *Arabidopsis* (Berná et al., 1999), we identified the recessive *ron1-1* mutation, which causes vegetative leaves to be rounded and increases leaf palisade mesophyll cell size. Mutants with fewer but enlarged cells, such as *ron1-1*, might provide insight into the intriguing phenomenon named compensation (Tsukaya, 2005). In addition, the *ron1-1* mutant exhibited an open venation pattern, which resulted from an increased number of free-ending veins. The pleiotropic phenotypes of *ron1-1* included late flowering, long root hairs, a reduced number of lateral roots, reduced inflorescence size, and increased inflorescence branching. Positional cloning demonstrated that *RON1* is identical to *SAL1* (Quintero et al., 1996), *FRY1* (Xiong et al., 2001), *HOS2* (Xiong et al., 2004), and *ALX8* (Wilson et al., 2009), which encodes an inositol polyphosphate 1-phosphatase. *FRY1* has been shown to rescue sulfur assimilation mutants in yeast (Quintero et al., 1996) and to negatively regulate ABA and stress signaling in *Arabidopsis* (Xiong et al., 2001, 2004). Mutations in *FRY1* are known to enhance the induction of stress genes in response to cold, ABA, salt, and dehydration and have been correlated with elevated levels of the IP_3 second messenger (Xiong et al., 2001). Additional roles for *FRY1* in the repression of drought tolerance and attenuation of light responses have recently been proposed (Kim and Von Arnim, 2009; Wilson et al., 2009). An analysis of the stromal proteome of *Arabidopsis* has shown that *FRY1* is localized to the chloroplast (Peltier et al., 2006). However, transient expression analysis of a *FRY1*-yellow fluorescent protein fusion in onion (*Allium cepa*) epidermal cells showed that *FRY1* is present in the nucleus and the cytoplasm (Kim and Von Arnim, 2009).

Effects of *ron1* Mutations on the *RON1/FRY1/SAL1* Protein

RON1/FRY1/SAL1/HOS2/ALX8 belongs to a group of evolutionarily related Li^+ - and Na^+ -sensitive and Mg^{2+} -dependent phosphatases (López-Coronado et al., 1999). The two phosphatase activities of *RON1/FRY1/SAL1* reside in its PAP phosphatase domain. The inositol polyphosphate 1-phosphatase activity is proposed to mediate IP_3 breakdown by dephosphorylating the inositol 1,4-bisphosphate and inositol 1,3,4-trisphosphate intermediates (Majerus, 1992). The activity of *RON1/FRY1/SAL1* against these two intermediates has been shown in vitro (Quintero et al., 1996). Additionally, *FRY1* demonstrates low in vitro activity against IP_3 , which is lost in the *FRY1-1* mutant protein (Xiong et al., 2001). Consistent with the role of *RON1/FRY1/SAL1* in IP_3 breakdown, the *fry1-1* mutant has increased endogenous IP_3 levels (Xiong et al., 2001).

As a nucleotidase, *RON1/FRY1/SAL1* displays in vitro activity against PAP, 2'-phosphoadenosine

5'-phosphate, and 3'-phosphoadenosine 5'-phosphosulfate, and this activity can rescue sulfate assimilation in *met22/hal2* yeast mutants (Quintero et al., 1996). The *fry1* mutants, like *ron1* mutants, grow appropriately using inorganic sulfate as the sole sulfur source and do not show any visible symptoms of sulfur deficiency (Xiong et al., 2001). Moreover, RON1/FRY1/SAL1 homologs mainly function as inositol phosphatases in multicellular organisms. These two facts led Xiong and colleagues (2001) to propose that RON1/FRY1/SAL1 is an inositol polyphosphate 1-phosphatase that mediates IP₃ catabolism and participates in the PI signaling pathway.

The insertional allele of *RON1/FRY1/SAL1*, *ron1-2*, is likely to be null because it is predicted to produce a protein lacking 282 amino acids. The similar leaf shape and vein-patterning phenotypes of *ron1-1* suggest that it is also null. *fry1-1* has also been proposed to be a null allele because it results in the absence of the α -5 helix in the mutant protein (Xiong et al., 2001). The leaves of *fry1-1* and *fry1-2* are more serrated than those of their corresponding wild type (C24; Xiong et al., 2001), a trait that is also observed for the *ron1-2* mutant (in the Col-0 background) but not for *ron1-1* (*Ler*), suggesting that this trait is suppressed in the *Ler* background.

A Role for RON1 in Vein Patterning

The role of inositol in vascular development was first revealed by cloning of *CVP2*, which encodes an inositol 5PTase (Carland and Nelson, 2004), and subsequently confirmed by cloning of *At5PTase13*, which encodes a different 5PTase enzyme (Lin et al., 2005). The similar vascular phenotypes of *cvp2*, *at5ptase13*, and *ron1* mutants suggest that inositol signaling is critical for vascular patterning. The distinct effects of *cvp2* and *ron1* mutations on leaf development suggest that different inositol metabolites participate in distinct developmental processes or, alternatively, that some phenotypic traits that are visible in *ron1* mutants, such as the rounded leaves, are masked in *cvp2* mutants by the presence of a redundant 5PTase activity. Indeed, as many as 15 5PTases are encoded in the Arabidopsis genome (Carland and Nelson, 2004), and one of them, *CVL1*, has been shown to act with *CVP2* to determine vein continuity. While *cvp2* mutants only show free-ending veins restricted to leaf and cotyledon margins, and *cvl1* mutants do not show any vascular defect, *cvp2 cvl1* double mutants also have vein islands, which are not seen in either single mutant (Carland and Nelson, 2009; Naramoto et al., 2009). Our results suggest that *cvp2-1* is epistatic on *ron1-2* as regards the formation of free-ending veins, since this trait was similar to *cvp2-1* in *ron1-2 cvp2-1* double mutants. However, *ron1-2 cvp2-1* double mutants also showed a slight, but statistically significant, reduction in venation density compared with the single mutants, which resemble the wild type in this parameter, suggesting that the inositol polyphosphate 1-phosphatase activity of RON1 can compensate for the reduction of

5PTase activity in *cvp2-1* mutants to some extent regarding this trait.

An interplay between inositol metabolism and auxin perception is indicated by the altered expression patterns of the *DR5-GUS* reporter in *cvp2* and *at5ptase13* mutants as well as by the altered expression levels of auxin-responsive genes in *at5ptase13* (Carland and Nelson, 2004; Lin et al., 2005). Although *DR5-GUS* is often presented as being a reporter of the auxin concentration, it is more accurately described as a reporter of auxin perception. *DR5* is an artificial promoter that includes tandemly repeated auxin response elements, known binding sites for auxin response factors (ARFs; Ulmasov et al., 1997). The auxin receptor was identified as the F-box protein TIR1 (Dharmasiri et al., 2005; Kepinski and Leyser, 2005), a component of the SCF^{TIR1} ubiquitin ligase complex. Binding of auxin to TIR1 leads to the ubiquitination and proteolytic degradation of members of a family of short-lived Aux/IAA proteins via the proteasome. In the absence of auxin, Aux/IAA proteins titrate ARF transcriptional repressors, preventing their binding to auxin response element-containing promoters and thus allowing transcription. Therefore, reduced expression levels of *DR5-GUS* may reflect low auxin concentrations, the inability to perceive auxin, or a failure to degrade Aux/IAA proteins. Conversely, elevated expression levels of *DR5-GUS* may translate into high auxin concentrations, active auxin perception, or the degradation of Aux/IAA proteins.

Based on our phenotypic observations of *ron1* mutants and on the synergistic phenotypes of *ron1 axr1* and *ron1 hve* double mutants, we hypothesize that inositol compounds function to modulate auxin perception. The mechanism for this modulation is unknown at present, but the presence of a myoinositol 1,2,3,4,5,6-hexakisphosphate (also known as IP₆ and phytate) molecule in the structure of the SCF^{TIR1} ubiquitin ligase complex bound to auxin (Tan et al., 2007) indicates that the interaction might be direct. Inositol hexakisphosphate has been proposed to be a structural cofactor in the SCF^{TIR1} complex. Negative charges provided by the phosphates in inositol hexakisphosphate are important in the interaction with positively charged residues in TIR1 (Tan et al., 2007).

Our results provide genetic evidence that loss-of-function mutations in *RON1*, which affect inositol phosphorylation, dramatically enhance the phenotypes of double mutants with *axr1* or *hve*. It has been suggested that the dynamics of highly phosphorylated inositols, such as IP₆ or IP₅, may be altered in *ron1* mutants (Xiong et al., 2001). *AXR1* is required for the neddylation of CULLIN1 (*CUL1*), one of the core components of the SCF^{TIR1} complex. *HVE* encodes *CAND1*, a protein that physically interacts with unneddylated *CUL1* to regulate the formation and/or the function of SCF complexes (Chuang et al., 2004; Feng et al., 2004; Alonso-Peral et al., 2006). Loss-of-function alleles of *AXR1* and *HVE* lead to similarly reduced venation patterns in which most tertiary and higher

order veins are absent, highlighting the importance of auxin perception for vascular patterning (Alonso-Peral et al., 2006; Candela et al., 2007). These phenotypes closely resemble those caused by loss-of-function alleles of *YUCCA* genes in triple or quadruple mutant combinations in *Arabidopsis* (Cheng et al., 2006). *YUCCA* proteins are flavin monooxygenases, key enzymes in Trp-dependent auxin biosynthesis (Zhao et al., 2001; Cheng et al., 2006). In our study, the enhanced *axr1* and *hve* mutant phenotypes caused by *ron1* alleles led to extremely simple, completely open vascular networks and to deeply lobed leaf laminae. Indeed, some pleiotropic traits in *ron1-1* are reminiscent of a mild defect in auxin perception. The increased branching of *ron1-1* shoots, although clearly distinct from the severe effects of *axr1* and *hve* mutations on inflorescence branching, may also result from a decrease in apical dominance due to defective auxin perception. In line with this idea, increased shoot branching has recently been described for plants that overexpress an inositol polyphosphate 6-/3-kinase gene (Zhang et al., 2007). Although our assays did not allow us to detect changes in sensitivity to 2,4-D, those authors found that these overexpressors are less sensitive to IAA than the wild type (Zhang et al., 2007).

Alternatively, it is also possible that the effect of *ron1* mutations on auxin responses results from a perturbation of auxin transport. This idea is not necessarily in disagreement with changes in auxin perception. Recently, a role of CVP2 in PIN1 trafficking has been described (Carland and Nelson, 2009; Naramoto et al., 2009). In addition to its activity on soluble forms of IP, CVP2 can generate phosphatidylinositol 4-monophosphate (Carland and Nelson, 2009), a specific PI ligand of SFC/VAN3 (Koizumi et al., 2005), an ARF-GAP protein involved in the cell polar localization of PIN1 through vesicle transport (Koizumi et al., 2005; Sieburth et al., 2006). Leaves of the *cvp2 cvl1* double mutant show open vein patterns similar to the ones observed in the leaves of *sfc* (Carland and Nelson, 2009; Naramoto et al., 2009). The function of at least one of these 5-phosphatases is necessary for the correct subcellular localization of VAN3 (Naramoto et al., 2009), which in turn affects vesicle transport and therefore PIN1 polar localization. To our knowledge, no inositol polyphosphate 1-phosphatase activity against PIs has been described so far. However, we cannot rule out that changes in inositol metabolism due to *ron1* mutations affect PI metabolism and alter vesicle trafficking. In fact, our double mutant analysis suggests that *cvp2-1* is epistatic to *ron1-2* for some aspects of vein patterning, suggesting that they act in the same developmental pathway. Future analyses involving genetic interactions between *ron1* and *van3/sfc* mutations and PIN1 subcellular localization will shed light on this issue.

Our *ron1-1* transcriptomic analysis did not reveal changes in genes previously described to participate in vein patterning, potentially suggesting that the re-

quirement for *RON1* activity in vein development functions downstream of these genes. However, one of the most down-regulated genes in the *ron1-1* microarray was *GH3.3* (At2g23170; 0.36-fold change), which encodes an enzyme that conjugates IAA in vitro to different amino acids, such as Asp (Staswick et al., 2005). Plants may regulate the effects of auxin through the production of different IAA-amido conjugates. In fact, because Asp is one of the amino acids that can be conjugated to auxin with high efficiency in vitro, and because IAA-Asp is a target for auxin degradation (Ljung et al., 2002), the formation of IAA-Asp may result in decreased active IAA levels. Moreover, *GH3.3* is highly up-regulated after IAA treatment (Nemhauser et al., 2006), which may reflect the need for the plant to remove excess auxin. The down-regulated expression of *GH3.3* in *ron1-1* would have the opposite effect: the reduced auxin response in some parts of the mutant may be counteracted by a reduction in the removal of this hormone in an attempt to maintain the correct developmental program controlled by free auxin. Besides, IAA-amido conjugates and IAA-ester conjugates, such as IAA-myoinositol and IAA-myoinositol glucosides, have also been described in plants and may contribute to regulate IAA levels (Ljung et al., 2002), since these ester forms of IAA constitute a storage form of auxin. Changes in the metabolism of inositol may cause an imbalance in the levels of different inositol compounds, which in turn may affect the levels of different inositol conjugates, such as IAA-inositol esters.

Plants produce IAA through different pathways, including Trp-dependent and Trp-independent pathways. Our metabolomic analysis revealed an increase in the levels of indole-3-acetonitrile, a precursor of IAA biosynthesis (Bartling et al., 1994). In line with this result, our transcriptomic analysis showed the down-regulation of a gene encoding a putative nitrilase (At4g08790), an enzyme that might catalyze to some extent the conversion of indole-3-acetonitrile into IAA (Piotrowski, 2008). Although we did not detect any change in the levels of Trp, those of shikimate, one of its precursors, were increased. Thus, we cannot rule out that the poor auxin response in the *ron1-1* mutant may be due to some extent to an imbalance in auxin levels.

Pleiotropy of *ron1* Mutants

It is likely that loss of function of *FRY1* restores posttranscriptional gene silencing in the *argonaute1-27* (*ago1-27*) and *ago1-33* backgrounds by corepressing the XRN2, XRN3, and XRN4 exoribonucleases, which in turn increases RNA-silencing triggers (Gy et al., 2007). The same authors found similar levels of the full-length mRNAs of the miR160 target genes *ARF10*, *ARF16*, and *ARF17* in *fry1* mutant and control plants. However, increased levels of the 3' products of the miRNA-guided cleavage products of these genes were found in the *fry1* mutant background, probably as a

result of inhibition of the cytoplasmic exoribonuclease XRN4 by PAP. In contrast to these results, our microarray analysis revealed increased levels of *ARF10*, *ARF16*, and *ARF17* mRNAs in *ron1-1*. It is possible that we detected the accumulation of 3' cleavage products from miRNA target genes in *ron1-1* because the probe sets in the ATH1 array were designed using the last 600 bp of the coding sequence (Redman et al., 2004). This premise could explain the apparently contradictory results and should make us cautious about interpreting microarray results involving miRNA target genes. In fact, although we found expression changes in 24 miRNA target genes, it is still possible that the transcription of most of these genes remains unchanged in the *ron1-1* background, since, for 17 of them, the probes in the ATH1 microarray were designed downstream of their miRNA cleavage sites.

In an ATH1 microarray analysis performed on leaf RNA from the *fry1-1* and *alx8* mutants, which carry alleles of *RON1*, a total of 2,447 and 1,844 were found to be deregulated (Wilson et al., 2009), in contrast with the 663 genes that we found in *ron1-1*. These differences may be due to the different experimental setup; while Wilson et al. (2009) used 5-week old green leaves from plants grown on soil, we used shoot apices (comprising shoot apical meristem and first and second leaf primordia at the petioleless stage, between 7 and 9 DAS) of seedlings grown on Murashige and Skoog (MS) medium containing Suc. We compared the three microarray analyses and found in common 142 up-regulated and 35 down-regulated genes. We did not detect changes in the expression of genes known to participate in vein patterning in the microarray data set of Wilson et al. (2009). However, two auxin transporters are down-regulated in these mutants: *PIN7* in *alx8* and *fry1-1* and *PIN4* in *alx8* (Feraru and Friml, 2008).

It is possible that perturbations in the homeostasis of a main signaling molecule such as IP_3 affect a number of developmental, response, and metabolic processes. For example, one of the most conspicuous developmental phenotypic traits of *ron1* mutants is late flowering. In the *ron1-1* microarray, overexpression of *CCA* and *LHY*, two genes encoding MYB-related transcription factors that are part of the Arabidopsis core oscillator, was detected, and constitutive overexpression of *CCA1* and gain-of-function alleles of *LHY* have been shown to cause late flowering (Schaffer et al., 1998; Wang and Tobin, 1998). Thus, it is plausible that the delayed flowering observed for *ron1* mutants is caused, to some extent, by the up-regulated expression of these two genes. Moreover, overexpression of *CCA1* disrupts circadian gene expression, which may be responsible for the *ron1-1* microarray enrichment for down-regulated genes including in their promoters the evening element, which is present in genes with circadian rhythmic expression (Harmer et al., 2000). Since IP_3 triggers Ca^{2+} release from intracellular stores (Tang et al., 2007) and since Ca^{2+} levels oscillate daily, probably encoding circadian clock signaling infor-

mation (Johnson et al., 1995; Love et al., 2004), it is possible that the altered IP_3 homeostasis in the *ron1-1* mutant causes changes in the oscillator, resulting in abrogated rhythmic gene expression and changes in light and metabolic pathways that are typically synchronized with day/night cycles. The involvement of *RON1* in the attenuation of light responses through its 3'(2'),5'-bisphosphate nucleotidase activity has been recently described (Kim and Von Arnim, 2009). In this study, late flowering under long-day conditions (16 h of light, 8 h of dark) has been related to the photoperiodic control of flowering, since low levels of *FLOWERING LOCUS T (FT)* mRNA are observed in the *fry1-6* mutant. Our transcriptomic analysis did not reveal any change in *FT* transcription in *ron1-1*, probably due to the different experimental conditions.

The characterization of *ron1* suggests that inositol compounds participate in a number of plant developmental processes. Further experiments will help us better understand the interplay between inositol metabolism and auxin responses and the regulatory roles of inositol in plant biology.

MATERIALS AND METHODS

Plant Material and Growth Conditions

The *Ler* and Col-0 wild-type accessions of Arabidopsis (*Arabidopsis thaliana*), the *axr1-12* (N3076; Leyser et al., 1993) and *hve-2* (SALK_099479; Alonso-Peral et al., 2006) mutants, both in the Col-0 background, as well as the SALK_005741, SALK_079259, and SALK_020882 T-DNA insertion lines from the Salk Institute Genome Analysis Laboratory (Alonso et al., 2003) were obtained from the Nottingham Arabidopsis Stock Centre. Additional insertion lines used in this work include SALK_142613, SALK_101314, SALK_101315, and SALK_101324 (At5g64000; *SAL2*); SALK_065642, SAIL_1160_G06, and SAIL_390_C04 (At5g63990; *SAL3*); SALK_101811, SALK_085187, SALK_085091, SAIL_252_C08, and GT_5.45527 (At5g09290; *SAL4*); and SALK_150680, SALK_055685, SALK_039705, and SALK021397 (At5g54390; *AHL*), all of which were obtained from the Nottingham Arabidopsis Stock Centre. The strong *cyp1-3* and *cyp2-1* loss-of-function mutants in the Col-0 background were kindly provided by Francine Carland (Carland et al., 1999). The transgenic *DR5-GUS* (Col-0 background) and *ATHB8-GUS* (Wassilewskija background) reporter lines were kindly provided by Thomas Guilfoyle and Simona Baima, respectively. All double mutant combinations were made using alleles in the Col-0 background and are homozygous unless otherwise stated.

For morphometric, metabolomic, and physiological assays, plants were grown on agar medium at $20^\circ\text{C} \pm 1^\circ\text{C}$ and 60% to 70% relative humidity under 5,000 lux continuous fluorescent light (Ponce et al., 1998). Crosses and allelism tests were carried out as described previously (Berná et al., 1999). For microarray analysis, the medium contained half-strength MS salts (microelements and macroelements), 1 g L^{-1} Suc, 0.5 g L^{-1} MES, pH 6.0, and 6 g L^{-1} plant tissue culture agar. Sixty seeds were sown per $150 \times 25\text{-mm}$ round petri dish, and the dishes were sealed with Urgopore tape and incubated in the dark at 4°C for 3 d. The growth chamber conditions were 16/8 h (day/night) with white light (neon tubes, cool-white), $100\ \mu\text{E m}^{-2}\text{ s}^{-1}$ photosynthetically active radiation, and 20°C .

Morphometric and Histological Analyses

Morphometric analyses of leaf venation patterns were performed at 22 DAS for cotyledons and leaves of *ron1-1* and *Ler* and 21 DAS for the comparisons of wild-type, single mutant, and double mutant strains in the Col-0 background. Leaf clearing, venation pattern visualization, and morphometry were performed as described by Alonso-Peral et al. (2006). The

number of free-ending veins was determined manually based on drawings of cotyledon and leaf venation patterns.

For the detection of GUS activity, plant tissue was incubated in 90% acetone on ice for 15 min and then in X-Gluc buffer solution (2 mM 5-bromo-4-chloro-3-indolyl- β -glucuronic acid, 50 mM sodium phosphate, pH 7.2, 5 mM potassium ferrocyanide, 50 mM potassium ferricyanide, and 0.2% Triton X-100) for 14 h at 37°C. After GUS detection, the tissue was cleared through an ethanol series (70%, 80%, 90%, and 96%) and mounted in an 8:2:1 (chloral hydrate:glycerol:water) solution.

To determine palisade mesophyll cell size, six first-node leaves of *Ler* and *ron1-1* plants grown in vitro were harvested at 23 DAS. Leaves were cleared with chloral hydrate, and the palisade mesophyll was visualized using differential interference contrast optics and photographed at the widest part of the lamina. Cell size was scored using NIS Elements (Nikon Imaging).

Statistical Analyses

Unless otherwise stated, we tested the normality of our data sets using nonparametric Kolmogorov-Smirnov tests. For data sets comprising two independent samples with 10 or more normally distributed values, the statistical significance of the mean differences of both samples was analyzed using Student's *t* test. For data sets comprising fewer than 10 values in one or both samples, we employed the Mann-Whitney *U* test. The analyses were carried out using SPSS 10.0.5 software (SPSS Inc.).

Map-Based Cloning

DNA extraction, amplified fragment length polymorphism, insertion/deletion, and single-nucleotide polymorphism analyses were performed according to Peters et al. (2004) and Cnops et al. (2004). Fine-mapping of the *RON1* locus was conducted using the markers described in Supplemental Table S1. The seven candidate genes were amplified from genomic DNA and sequenced to identify the nucleotide substitution in *ron1-1* (Supplemental Table S2).

Physiological Assays

To study the effects of the auxin polar transport inhibitors NPA and TIBA and the synthetic auxin 2,4-D on root elongation, seedlings were grown on vertically oriented MS agar plates supplemented with different concentrations of NPA (1, 5, and 10 μ M), TIBA (1 and 10 μ M), or 2,4-D (10, 50, 100, 200, 500, and 1,000 mM). NPA and 2,4-D were added from stock solutions dissolved in dimethyl sulfoxide and NaOH, respectively. To determine root growth inhibition in the presence of NPA, the primary roots of over 50 seedlings were measured at 7 DAS. For the 2,4-D treatments, seedlings grown on vertically oriented MS agar plates were transferred at 5 DAS to plates containing 2,4-D, and the primary roots of 15 or more seedlings were measured 5 d later.

To study the effects of 2,4-D and IAA on the expression of the *DR5-GUS* transgene, plants grown on agar medium were incubated for 6 h in scintillation vials containing liquid medium supplemented with 1 μ M 2,4-D or IAA and subsequently stained for GUS activity as described previously (Alonso-Peral et al., 2006).

Microarray Preparation, Hybridization, and Data Analysis

The microarray experiment, including RNA extraction, experimental design, and data analysis, was processed as described by Fleury et al. (2007) using ATH1 Affymetrix chips of Arabidopsis, Bioconductor Project Release 1.4 (Gentleman et al., 2004) and BiNGO version 2 (Maere et al., 2005) software. The false discovery rate method for multiple testing was used to correct the *P* value of the Bayesian *t* test. The differentially expressed genes between the wild type and the mutant were selected at *P* < 0.01. Since some microarray elements of ATH1 match more than one annotated gene (Arabidopsis Genome Initiative code), we used the list of all annotated genes in the Gene Ontology analysis (BiNGO). The data are available on ArrayExpress (E-TAMB-566).

RT-PCR, qRT-PCR, and Microarray in Silico Analysis

Primers F (5'-TCGCTGCTCGTCTCTGTCAG-3') and R (5'-GTTTGGACAAGCAAGCACACC-3') were used to detect alternatively spliced tran-

script forms in the *ron1-1* mutant. The expression pattern of *RON1* was studied using the Gene Atlas and Gene Chronologer options in Genevestigator (Zimmermann et al., 2005).

Aliquots of the RNA samples used for the microarray analysis were employed as templates for qRT-PCR validation. Two micrograms of mRNA was heated for 5 min at 65°C and immediately transferred to ice, followed by addition of 500 ng of 10Xp(dN)₆ primers (Boehringer Mannheim) and incubation of the mixture at room temperature for 10 min. cDNA synthesis was performed in a 40- μ L reaction mixture containing 0.5 mM of each deoxyribonucleotide triphosphate, 10 mM dithiothreitol, 200 units of SuperScript II enzyme (Gibco BRL), and 40 units of RNaseOUT. After cDNA synthesis, 80 μ L of RNase-free water was added to the reaction mixture. One microliter of the resulting cDNA solution was used for qRT-PCR amplifications, which were carried out in an ABI PRISM 7000 sequence detection system (Applied Biosystems) as described by Pérez-Pérez et al. (2004). Primer pairs (Supplemental Table S4) were designed to yield amplification products of approximately 100 bp. When possible, at least one primer of each primer pair contained sequences complementary to the ends of two contiguous exons, so that genomic DNA could not be amplified. Each 25- μ L reaction mix contained 12.5 μ L of the SYBR-Green PCR Master Mix (Applied Biosystems), 0.4 μ M of primers, and 1 μ L of cDNA solution. Relative quantification of the gene expression data was performed using the 2^{- $\Delta\Delta$ CT} or comparative C_T method (Livak and Schmittgen, 2001). Each reaction was performed in triplicate, and expression levels were normalized using the C_T values obtained for the *OTC* housekeeping gene (Quesada et al., 1999).

To compare the *ron1-1* microarray data set with that of Nemhauser et al. (2006), a binomial sampling distribution was used (*P* < 0.05). To analyze gene promoters, we used the Athena Web-based application, which includes a database containing 30,067 predicted promoter sequences from Arabidopsis together with consensus sequences for 105 characterized transcription factor binding sites. The significance of enrichment (*P* value) for specific sequences was calculated using a hypergeometric probability distribution with Bonferroni correction (<http://www.bioinformatics2.wsu.edu/cgi-bin/Athena/cgi/home.pl>; O'Connor et al., 2005).

Metabolite Data

Extraction and derivatization of metabolites from third and fourth leaves of plants collected at 21 DAS using GC-MS were performed as outlined by Lisec et al. (2006). GC-MS data were obtained using an Agilent 7683 series autosampler (Agilent Technologies) coupled to an Agilent 6890 gas chromatograph coupled to a Leco Pegasus 2 time-of-flight mass spectrometer (LECO). Identical chromatogram acquisition parameters were used as those described previously (Weckwerth et al., 2004). Chromatograms were exported from Leco ChromaTOF software (version 3.25) to R software. An in-house R script was employed to perform peak detection, retention time alignment, and library matching. Metabolite data were normalized by dividing each raw value by the median of all measurements of the experiment for one metabolite. To calculate the significant changes in the profiles of *ron1-1* and the wild type, *t* tests with false discovery rate correction were performed using R software.

Supplemental Data

The following materials are available in the online version of this article.

Supplemental Figure S1. The *ron1-2* mutant.

Supplemental Figure S2. Expression of *DR5-GUS* in *ron1-1* and wild-type plants incubated with auxin.

Supplemental Figure S3. Rosette phenotype of double mutants.

Supplemental Figure S4. Synergistic phenotypes in *ron1-2 hve-2* double mutant.

Supplemental Figure S5. Metabolic changes of *ron1-1* relative to *Ler*.

Supplemental Table S1. Molecular markers used for the fine-mapping of *RON1*.

Supplemental Table S2. Candidate genes within the 30-kb interval defined by fine-mapping of *RON1*.

Supplemental Table S3. Microarray analysis of *ron1-1* apices.

Supplemental Table S4. Primers used for qRT-PCR validation of microarray results.

Supplemental Table S5. qRT-PCR validation of microarray results.

Supplemental Table S6. BiNGO analysis of the differentially expressed genes in the *ron1-1* microarray.

Supplemental Table S7. miRNA target genes found in the *ron1-1* microarray.

Supplemental Table S8. Behavior of hormone transcriptional targets in *ron1-1*.

Supplemental Table S9. Down-regulated genes in the *ron1-1* microarray containing the evening element in their promoters.

Supplemental Table S10. Down-regulated genes in the *ron1-1* microarray encoding chloroplast-targeted proteins.

Supplemental Table S11. Relative metabolite contents of *ron1-1* leaves.

ACKNOWLEDGMENTS

We thank J.M. Serrano, V. García, T. Trujillo, S. De Block, P. Van Hummelen, A. Eckardt, and the technicians of the MicroArrays Facility (Leuven, Belgium) for technical assistance, the Salk Institute Genomic Analysis Laboratory for the sequence-indexed *Arabidopsis* T-DNA insertion mutants, Francine Carland for the *cvp1-3* and *cvp2-1* mutants, and Thomas Guilfoyle for the *DR5-GUS* line.

Received October 13, 2009; accepted December 26, 2009; published December 31, 2009.

LITERATURE CITED

- Alonso JM, Stepanova AN, Leisse TJ, Kim CJ, Chen H, Shinn P, Stevenson DK, Zimmerman J, Barajas P, Cheuk R, et al (2003) Genome-wide insertional mutagenesis of *Arabidopsis thaliana*. *Science* **301**: 653–657
- Alonso-Peral MM, Candela H, del Pozo JC, Martínez-Laborda A, Ponce MR, Micol JL (2006) The *HVE/CAND1* gene is required for the early patterning of leaf venation in *Arabidopsis*. *Development* **133**: 3755–3766
- Baima S, Nobili F, Sessa G, Lucchetti S, Ruberti I, Morelli G (1995) The expression of the *Athb-8* homeobox gene is restricted to provascular cells in *Arabidopsis thaliana*. *Development* **121**: 4171–4182
- Bartling D, Seedorf M, Schmidt RC, Weiler E (1994) Molecular characterization of two cloned nitrilases from *Arabidopsis thaliana*: key enzymes in biosynthesis of the plant hormone indole-3-acetic acid. *Proc Natl Acad Sci USA* **91**: 6021–6025
- Berná G, Robles P, Micol JL (1999) A mutational analysis of leaf morphogenesis in *Arabidopsis thaliana*. *Genetics* **152**: 729–742
- Berridge MJ (2009) Inositol trisphosphate and calcium signalling mechanisms. *Biochim Biophys Acta* **1793**: 933–940
- Candela H, Alonso-Peral MM, Ponce MR, Micol JL (2007) Role of *HEMIVENATA* and the ubiquitin pathway in venation pattern formation. *Plant Signal Behav* **2**: 258–259
- Candela H, Martínez-Laborda A, Micol JL (1999) Venation pattern formation in *Arabidopsis thaliana* vegetative leaves. *Dev Biol* **205**: 205–216
- Carland E, Nelson T (2009) CVP2- and CVL1-mediated phosphoinositide signaling as a regulator of the ARF GAP SFC/VAN3 in establishment of foliar vein patterns. *Plant J* **59**: 895–907
- Carland FM, Berg BL, FitzGerald JN, Jinamornphongs S, Nelson T, Keith B (1999) Genetic regulation of vascular tissue patterning in *Arabidopsis*. *Plant Cell* **11**: 2123–2137
- Carland FM, Fujioka S, Takatsuto S, Yoshida S, Nelson T (2002) The identification of *CVP1* reveals a role for sterols in vascular patterning. *Plant Cell* **14**: 2045–2058
- Carland FM, Nelson T (2004) *COTYLEDON VASCULAR PATTERN2*-mediated inositol (1,4,5) triphosphate signal transduction is essential for closed venation patterns of *Arabidopsis* foliar organs. *Plant Cell* **16**: 1263–1275
- Cheng Y, Dai X, Zhao Y (2006) Auxin biosynthesis by the YUCCA flavin monooxygenases controls the formation of floral organs vascular tissues in *Arabidopsis*. *Genes Dev* **20**: 1790–1799
- Chuang HW, Zhang W, Gray WM (2004) *Arabidopsis* ETA2, an apparent ortholog of the human cullin-interacting protein CAND1, is required for auxin responses mediated by the SCF(TIR1) ubiquitin ligase. *Plant Cell* **16**: 1883–1897
- Cnops G, Jover-Gil S, Peters JL, Neyt P, De Block S, Robles P, Ponce MR, Gerats T, Micol JL, Van Lijsebettens M (2004) The *rotunda2* mutants identify a role for the *LEUNIG* gene in vegetative leaf morphogenesis. *J Exp Bot* **55**: 1529–1539
- Cnops G, Neyt P, Raes J, Petrarulo M, Nelissen H, Malenica N, Luschnig C, Tietz O, Ditengou F, Palme K, et al (2006) The *TORNADO1* and *TORNADO2* genes function in several patterning processes during early leaf development in *Arabidopsis thaliana*. *Plant Cell* **18**: 852–866
- De Smet I, Jürgens G (2007) Patterning the axis in plants: auxin in control. *Curr Opin Genet Dev* **17**: 337–343
- Deyholos MK, Cavaness GF, Hall B, King E, Punwani J, Van Norman J, Sieburth LE (2003) VARICOSE, a WD-domain protein, is required for leaf blade development. *Development* **130**: 6577–6588
- Deyholos MK, Cordner G, Beebe D, Sieburth LE (2000) The *SCARFACE* gene is required for cotyledon leaf vein patterning. *Development* **127**: 3205–3213
- Dharmasiri N, Dharmasiri S, Estelle M (2005) The F-box protein TIR1 is an auxin receptor. *Nature* **435**: 441–445
- Evert RE, Eichhorn SE (2006) *Esau's Plant Anatomy. Meristems, Cells, and Tissues of the Plant Body: Their Structure, Function, and Development*, Ed 3. John Wiley & Sons, Hoboken, NJ
- Feng S, Shen Y, Sullivan JA, Rubio V, Xiong Y, Sun TP, Deng XW (2004) *Arabidopsis* CAND1, an unmodified CUL1-interacting protein, is involved in multiple developmental pathways controlled by ubiquitin/proteasome-mediated protein degradation. *Plant Cell* **16**: 1870–1882
- Feraru E, Friml J (2008) PIN polar targeting. *Plant Physiol* **147**: 1553–1559
- Fleury D, Himanen K, Cnops G, Nelissen H, Boccardi TM, Maere S, Beemster G, Anami S, Neyt P, Robles P, et al (2007) The *Arabidopsis* homolog of yeast *BRE1* has a function in cell cycle regulation during early leaf root growth. *Plant Cell* **19**: 417–432
- Gälweiler L, Guan C, Muller A, Wisman E, Mendgen K, Yephremov A, Palme K (1998) Regulation of polar auxin transport by AtPIN1 in *Arabidopsis* vascular tissue. *Science* **282**: 2226–2230
- Gentleman RC, Carey VJ, Bates DM, Bolstad B, Dettling M, Dudoit S, Ellis B, Gautier L, Ge Y, Gentry J, et al (2004) Bioconductor: open software development for computational biology and bioinformatics. *Genome Biol* **5**: R80
- Gy I, Gascioli V, Lauressergues D, Morel JB, Gombert J, Proux F, Proux C, Vaucheret H, Mallory AC (2007) *Arabidopsis* FIERY1, XRN2, XRN3 are endogenous RNA silencing suppressors. *Plant Cell* **19**: 3451–3461
- Hardtke CS, Berleth T (1998) The *Arabidopsis* gene *MONOPTEROS* encodes a transcription factor mediating embryo axis formation and vascular development. *EMBO J* **17**: 1405–1411
- Harmer SL, Hogenesch JB, Straume M, Chang HS, Han B, Zhu T, Wang X, Kreps JA, Kay SA (2000) Orchestrated transcription of key pathways in *Arabidopsis* by the circadian clock. *Science* **290**: 2110–2113
- Hickey LJ (1973) Classification of the architecture of dicotyledonous leaves. *Am J Bot* **60**: 17–33
- Huang X, Madan A (1999) CAP3: a DNA sequence assembly program. *Genome Res* **9**: 868–877
- Johnson CH, Knight MR, Kondo T, Masson P, Sedbrook J, Haley A, Trewavas A (1995) Circadian oscillations of cytosolic chloroplastic free calcium in plants. *Science* **269**: 1863–1865
- Kepinski S, Leyser O (2005) The *Arabidopsis* F-box protein TIR1 is an auxin receptor. *Nature* **435**: 446–451
- Kim BH, Von Arnim AG (2009) *FIERY1* regulates light-mediated repression of cell elongation flowering time via its 3'-(2'),5'-bisphosphate nucleotidase activity. *Plant J* **58**: 208–219
- Koizumi K, Naramoto S, Sawa S, Yahara N, Ueda T, Nakano A, Sugiyama M, Fukuda H (2005) VAN3 ARF-GAP-mediated vesicle transport is involved in leaf vascular network formation. *Development* **132**: 1699–1711
- Krinke O, Novotná Z, Valentová O, Martinec J (2007) Inositol triphosphate receptor in higher plants: is it real? *J Exp Bot* **58**: 361–376
- Leyser HM, Lincoln CA, Timpte C, Lammer D, Turner J, Estelle M (1993) *Arabidopsis* auxin-resistance gene *AXR1* encodes a protein related to ubiquitin-activating enzyme E1. *Nature* **364**: 161–164
- Lin WH, Wang Y, Mueller-Roeber B, Brearley CA, Xu ZH, Xue HW (2005) At5PTase13 modulates cotyledon vein development through regulating auxin homeostasis. *Plant Physiol* **139**: 1677–1691
- Lisec J, Schauer N, Kopka J, Willmitzer L, Fernie AR (2006) Gas chroma-

- tography mass spectrometry-based metabolite profiling in plants. *Nat Protoc* 1: 387–396
- Livak KJ, Schmittgen TD (2001) Analysis of relative gene expression data using real-time quantitative PCR and the 2(-Delta Delta C(T)) method. *Methods* 25: 402–408
- Ljung K, Hul AK, Kowalczyk M, Marchant A, Celenza J, Cohen JD, Sandberg G (2002) Biosynthesis, conjugation, catabolism and homeostasis of indole-3-acetic acid in *Arabidopsis thaliana*. *Plant Mol Biol* 50: 309–332
- López-Coronado JM, Bellés JM, Lesage F, Serrano R, Rodríguez PL (1999) A novel mammalian lithium-sensitive enzyme with a dual enzymatic activity, 3'-phosphoadenosine 5'-phosphate phosphatase and inositol-polyphosphate 1-phosphatase. *J Biol Chem* 274: 16034–16039
- Love J, Dodd AN, Webb AA (2004) Circadian diurnal calcium oscillations encode photoperiodic information in *Arabidopsis*. *Plant Cell* 16: 956–966
- Maere S, Heymans K, Kuiper M (2005) BiNGO: a Cytoscape plugin to assess overrepresentation of Gene Ontology categories in biological networks. *Bioinformatics* 21: 3448–3449
- Majerus PW (1992) Inositol phosphate biochemistry. *Annu Rev Biochem* 61: 225–250
- Mattsson J, Ckurshumova W, Berleth T (2003) Auxin signaling in *Arabidopsis* leaf vascular development. *Plant Physiol* 131: 1327–1339
- Mattsson J, Sung ZR, Berleth T (1999) Responses of plant vascular systems to auxin transport inhibition. *Development* 126: 2979–2991
- Naramoto S, Sawa S, Koizumi K, Uemura T, Ueda T, Friml J, Nakano A, Fukuda H (2009) Phosphoinositide-dependent regulation of VAN3 ARF-GAP localization and activity essential for vascular tissue continuity in plants. *Development* 136: 1529–1538
- Nemhauser JL, Hong F, Chory J (2006) Different plant hormones regulate similar processes through largely nonoverlapping transcriptional responses. *Cell* 126: 467–475
- O'Connor TR, Dyreson C, Wyrick JJ (2005) Athena: a resource for rapid visualization systematic analysis of *Arabidopsis* promoter sequences. *Bioinformatics* 21: 4411–4413
- Okada K, Ueda J, Komaki M, Bell C, Shimura Y (1991) Requirement of the auxin polar transport system in early stages of *Arabidopsis* bud formation. *Plant Cell* 3: 677–684
- Ongaro V, Leyser O (2007) Hormonal control of shoot branching. *J Exp Bot* 59: 67–74
- Parker G, Schofield R, Sundberg B, Turner S (2003) Isolation of *COV1*, a gene involved in the regulation of vascular patterning in the stem of *Arabidopsis*. *Development* 130: 2139–2148
- Peltier JB, Cai Y, Sun Q, Zabrouskov V, Giacomelli L, Rudella A, Ytterberg AJ, Rutschow H, Van Wijk KJ (2006) The oligomeric stromal proteome of *Arabidopsis* chloroplasts. *Mol Cell Proteomics* 5: 114–133
- Pérez-Pérez JM, Candela H, Micol JL (2009) Understanding synergy in genetic interactions. *Trends Genet* 25: 368–376
- Pérez-Pérez JM, Ponce MR, Micol JL (2004) The *ULTRACURVATA2* gene of *Arabidopsis* encodes an FK506-binding protein involved in auxin brassinosteroid signaling. *Plant Physiol* 134: 101–117
- Peters JL, Cnops G, Neyt P, Zethof J, Cornelis K, Van Lijsebettens M, Gerats T (2004) An AFLP-based genome-wide mapping strategy. *Theor Appl Genet* 108: 321–327
- Piotrowski M (2008) Primary or secondary? Versatile nitrilases in plant metabolism. *Phytochemistry* 69: 2655–2667
- Pitts RJ, Cernac A, Estelle H (1998) Auxin and ethylene promote root hair elongation in *Arabidopsis*. *Plant J* 16: 553–560
- Ponce MR, Quesada V, Micol JL (1998) Rapid discrimination of sequences flanking and within T-DNA insertions in the *Arabidopsis* genome. *Plant J* 14: 497–501
- Przemeck GK, Mattsson J, Hardtke CS, Sung ZR, Berleth T (1996) Studies on the role of the *Arabidopsis* gene *MONOPTEROS* in vascular development and plant cell axialization. *Planta* 200: 229–237
- Quesada V, Ponce MR, Micol JL (1999) *OTC* and *AULL1*, two convergent and overlapping genes in the nuclear genome of *Arabidopsis*. *FEBS Lett* 461: 101–106
- Quintero FJ, Garcíadeblás B, Rodríguez-Navarro A (1996) The *SAL1* gene of *Arabidopsis*, encoding an enzyme with 3'(2'),5'-bisphosphate nucleotidase inositol polyphosphate 1-phosphatase activities, increases salt tolerance in yeast. *Plant Cell* 8: 529–537
- Redman JC, Haas BJ, Tanimoto G, Town CD (2004) Development evaluation of an *Arabidopsis* whole genome Affymetrix probe array. *Plant J* 38: 545–561
- Robles P, Micol JL (2001) Genome-wide linkage analysis of *Arabidopsis* genes required for leaf development. *Mol Genet Genomics* 266: 12–19
- Rolland-Lagan AG, Prusinkiewicz P (2005) Reviewing models of auxin canalization in the context of leaf vein pattern formation in *Arabidopsis*. *Plant J* 44: 854–865
- Roth-Nebelsick A, Uhl D, Mosbrugger V, Kerp H (2001) Evolution function of leaf architecture: a review. *Ann Bot (Lond)* 87: 553–566
- Sabatini S, Beis D, Wolkenfelt H, Murfett J, Guilfoyle T, Malamy J, Benfey P, Leyser O, Bechtold N, Weisbeek P, et al (1999) An auxin-dependent distal organizer of pattern polarity in the *Arabidopsis* root. *Cell* 99: 463–472
- Sachs T (1991) Cell polarity tissue patterning in plants. *Development* 113: 83–93
- Scarpella E, Marcos D, Friml J, Berleth T (2006) Control of leaf vascular patterning by polar auxin transport. *Genes Dev* 20: 1015–1027
- Schaffer R, Ramsay N, Samach A, Corden S, Putterill J, Carré IA, Coupland G (1998) The late elongated hypocotyl mutation of *Arabidopsis* disrupts circadian rhythms and the photoperiodic control of flowering. *Cell* 93: 1219–1229
- Sieburth LE (1999) Auxin is required for leaf vein pattern in *Arabidopsis*. *Plant Physiol* 121: 1179–1190
- Sieburth LE, Muday GK, King EJ, Benton G, Kim S, Metcalf KE, Meyers L, Seaman E, Van Norman JM (2006) *SCARFACE* encodes an ARF-GAP that is required for normal auxin efflux vein patterning in *Arabidopsis*. *Plant Cell* 18: 1396–1411
- Staswick PE, Serban B, Rowe M, Tiryaki I, Maldonado MT, Maldonado MC, Suza W (2005) Characterization of an *Arabidopsis* enzyme family that conjugates amino acids to indole-3-acetic acid. *Plant Cell* 17: 616–627
- Steyn QJ, Schultz EA (2003) The *FORKED* genes are essential for distal vein meeting in *Arabidopsis*. *Development* 130: 4695–4708
- Tan X, Calderon-Villalobos LI, Sharon M, Zheng C, Robinson CV, Estelle M, Zheng N (2007) Mechanism of auxin perception by the TIR1 ubiquitin ligase. *Nature* 446: 640–645
- Tang RH, Han S, Zheng H, Cook CW, Choi CS, Woerner TE, Jackson RB, Pei ZM (2007) Coupling diurnal cytosolic Ca²⁺ oscillations to the CAS-IP₃ pathway in *Arabidopsis*. *Science* 315: 1423–1426
- Tsukaya H (2005) Leaf shape: genetic controls and environmental factors. *Int J Dev Biol* 49: 547–555
- Ulmason T, Murfett J, Hagen G, Guilfoyle TJ (1997) Aux/IAA proteins repress expression of reporter genes containing natural highly active synthetic auxin response elements. *Plant Cell* 9: 1963–1971
- Wang ZY, Tobin EM (1998) Constitutive expression of the *CIRCADIAN CLOCK ASSOCIATED 1* (*CCA1*) gene disrupts circadian rhythms and suppresses its own expression. *Cell* 93: 1207–1217
- Weckwerth W, Wenzel K, Fiehn O (2004) Process for the integrated extraction, identification and quantification of metabolites, proteins and RNA to reveal their co-regulation in biochemical networks. *Proteomics* 4: 78–83
- Wilson P, Estavillo G, Field K, Pornsiriwong W, Carroll A, Howell K, Woo N, Lake J, Smith S, Harvey Millar A, et al (2009) The nucleotidase/phosphatase *SAL1* is a negative regulator of drought tolerance in *Arabidopsis*. *Plant J* 58: 299–317
- Xiong L, Lee B, Ishitani M, Lee H, Zhang C, Zhu JK (2001) *FIERY1* encoding an inositol polyphosphate 1-phosphatase is a negative regulator of abscisic acid stress signaling in *Arabidopsis*. *Genes Dev* 15: 1971–1984
- Xiong L, Lee H, Huang R, Zhu JK (2004) A single amino acid substitution in the *Arabidopsis* *FIERY1*/*HOS2* protein confers cold signaling specificity and lithium tolerance. *Plant J* 40: 536–545
- York JD, Ponder JW, Majerus PW (1995) Definition of a metal-dependent/Li(+)-inhibited phosphomonoesterase protein family based upon a conserved three-dimensional core structure. *Proc Natl Acad Sci USA* 92: 5149–5153
- Zhang ZB, Yang G, Arana F, Chen Z, Li Y, Xia HJ (2007) *Arabidopsis* inositol polyphosphate 6-/3-kinase (*AtIpk2β*) is involved in axillary shoot branching via auxin signaling. *Plant Physiol* 144: 942–951
- Zhao Y, Christensen SK, Fankhauser C, Cashman JR, Cohen JD, Weigel D, Chory J (2001) A role for flavin monooxygenase-like enzymes in auxin biosynthesis. *Science* 291: 306–309
- Zimmermann P, Hennig L, Gruißem W (2005) Gene-expression analysis and network discovery using Genevestigator. *Trends Plant Sci* 10: 407–409